POTENTIOMETER LAW MODELLING AND IDENTIFICATION FOR APPLICATION IN PHYSICS-BASED VIRTUAL ANALOGUE CIRCUITS

Ben Holmes and Maarten van Walstijn

Sonic Arts Research Centre,
School of Electronics, Electrical Engineering, and Computer Science,
Queen's University Belfast,
Belfast, UK
{ bholmes02@qub.ac.uk, m.vanwalstijn@qub.ac.uk }

ABSTRACT

Physical circuit models have an inherent ability to simulate the behaviour of user controls as exhibited by, for example, potentiometers. Working to accurately model the user interface of musical circuits, this work provides potentiometer 'laws' that fit to the underlying characteristics of linear and logarithmic potentiometers. A strategy of identifying these characteristics is presented, exclusively using input/output measurements and as such avoiding device disassembly. By breaking down the identification problem into one dimensional, search spaces characteristics are successfully identified. The proposed strategy is exemplified through a case study on the tone stack of the Big Muff Pi.

1. INTRODUCTION

Virtual Analogue (VA) modelling is largely motivated by the heritage aim of recreating analogue effects in functional digital form. A core component of an analogue effect is its user interface, i.e. the controls available to the musician to design and fine-tune the timbral qualities of the effect. To create a complete VA model of a device, its user interface must therefore also be carefully recreated.

A ubiquitous element of the user interface is found in potentiometers, which are present in countless guitar effects, synthesisers, etc. These devices map a change in rotation (or other movement) to a change in a specified phenomenon. Often, available schematics omit potentiometer laws, requiring a method of determining them from the circuit. Further, ideal laws that are commonly used may not truly reflect the behaviour of real potentiometers.

The aim of this paper is to investigate, identify, and model such mappings with a view of incorporating the resulting potentiometer laws into VA circuit models. Physical modelling is a good match for the overall simulation in this case, as it preserves the circuit topology, meaning that potentiometer changes result in local rather than global system changes. This does not hold for black- and grey-box models [1, 2], which focus on deriving a model for a single setting. A solution would require interpolation across a large number of coefficient data sets to facilitate such potentiometer control, equivalent to the strategy used to model a systems' response to changes in input signal amplitude [3].

The main advantage of black box models is that they are derived entirely from input/output (I/O) measurements, preventing the need to disassemble a device and so avoiding any risk of damage to the device under test. Previously it was found that for physical models, values of the components in a circuit can be identified using only I/O measurements and positioning potentiometers at the extreme ends of their travel [4]. The objective of this work is to complete a VA circuit model by identifying the underlying characteristic of a potentiometer, again only using I/O measurements. A key aspect of this challenge is to determine suitable fitting functions.

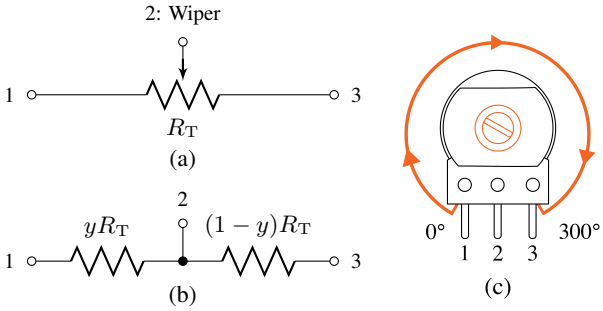

Figure 1: (a) *Annotated potentiometer schematic symbol.* (b) *Separation of the potentiometer symbol into the inter-terminal resistances as used to model its behaviour.* (c) *Rotary potentiometer diagram with labelled terminals, and the rotating shaft highlighted and range of rotation indicated, the shaft shown at 0 °.*

The rest of this paper is organised as follows: §2 investigates a variety of potentiometer laws and fits them to characteristics both from literature and also measurements of individual devices. §3 presents the identification strategy used to estimate potentiometer characterstics from I/O measurements, utilising the Big Muff Pi tone stack as a case study. §4 then presents the results of the characteristic identification from real I/O measurements, and finally §5 concludes the research and notes lines of future research. Companion material including MATLAB code and data sets are available online.[1]

2. MODELLING POTENTIOMETER CHARACTERISTICS

Potentiometers are a common component in musical circuits, used to provide a direct user interface. Some of the most common applications are for 'volume', 'tone', 'gain', etc. Illustrated in Figure 1, the potentiometer implements control over such quantities/phenomena by changing two resistances between three terminals relative to the position of its wiper which is actuated by the user.

The focus of this work is on how those resistances change with respect to a change in position of the wiper, referred to as its 'law'.

[1] https://bholmesqub.github.io/DAFx19/

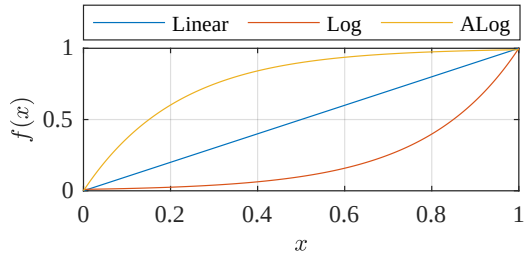

Figure 2: *Linear, logarithmic, and anti-logarithmic potentiometer tapers,* $\Delta_{\mathrm{dB}} = 40\,\mathrm{dB}$.

This law effectively maps the user's control to a change in the behaviour of the circuit, and is an essential feature of the user interface. Within the field of audio the most commonly encountered laws are linear and logarithmic, and will be the focus of the presented modelling and identification. Out of these two, it could be said that the logarithmic law is the most widely used, applied to map a linear control to logarithmic quantities such as loudness and frequency for application to volume controls and filter circuits.

2.1. Ideal laws

This section addresses 'ideal' potentiometer laws that are suitable for musical expression, but may not correspond exactly with how a physical potentiometer behaves electronically. An ideal potentiometer law is defined having a maximum total resistance R_{T} which is the sum of resistance between terminals 1 and 3 as illustrated in Figure 1. Each terminal and wiper are assumed to be perfect conductors i.e. have no resistance. Wiper position is defined here by the variable x which notes the rotation between terminals, and can be normalised such that $0 \leq x \leq 1$ which maps to a degree of total rotation usually between 0 and 300 degrees. The potentiometer law is defined as a function of the rotation, $y = f(x)$ which dictates the proportion of R_{T} that each resistor represents: $R_{1,2} = yR_{\mathrm{T}}$ and $R_{2,3} = (1-y)R_{\mathrm{T}}$, where subscript indicates terminal index. To reverse the orientation of the potentiometer the resistors change position between terminals, modelled as $y = 1 - f(x)$.

Ideal laws are shown in Figure 2, including an antilogarithmic law in addition to the previously mentioned linear and logarithmic laws. An ideal linear law can be defined as $f_{\mathrm{lin}}(x) = x$. A decibel ranged logarithmic function can be found by placing x in the exponent,

$$f_{\mathrm{log}}(x) = 10^{\frac{\Delta_{\mathrm{dB}}}{20}(x-1)}, \tag{1}$$

where Δ_{dB} is the desired range in decibels. This effectively maps linear rotation to a logarithmic law, a mapping which is used in other contexts for example in envelope design [5]. This law never reaches 0, which corresponds to $-\inf$ dB. Should a zero-value be desired the law can be translated and scaled, though it would then no longer be truly logarithmic.

The exponent operation can be computationally expensive depending on the system, and often approximations are offered such as a power law, e.g. $f(x) = x^4$ in [5]. Modern audio plug-in frameworks typically offer a variety of options to suit the needs of the developer [6].

An anti-logarithmic law is found by reflecting the logarithmic curve around $x = 0.5$ and $y = 0.5$, i.e. $f_{\mathrm{Alog}}(x) = \hat{f}_{\mathrm{log}}(x)$ where $\hat{f}(x) = 1 - f(1-x)$.

2.2. Laws from specifications

Though the ideal laws discussed in §2.1 may provide suitable control in software, these laws are unlikely to be encountered in real devices. In this section specifications are first investigated from a modelling perspective to determine which functions are suitable for capturing the behaviour of a real potentiometer law. Two functions are proposed to model the characteristics encountered in real devices, a $\tanh$ based function for broadly capturing multiple laws with a single function, and a piecewise function that aims to match the manufactured composition of the studied devices. The piecewise functions are then used to model measurements from real potentiometers that will then be used in the case study of the Big Muff Pi tone stack in §3.

To utilise data of potentiometer mapping characteristics shown in figures in the literature, online software for extracting data from images was used [7].

2.2.1. An analytic multi-law function

An authoritative source on potentiometers, 'The Potentiometer Handbook' [8] provides a reference for commonly occurring laws as well as the underlying manufacturing techniques behind them. The text refers to the Military Specification MIL-R-94B (now at revision G though characteristics are unaltered [9]), reproduced here in Figure 3. Each of these characteristics deviates from the ideal law, shown with gentle transitions towards the extreme ends of the functions. For the laws shown in Figure 3, a suitable non-piecewise function is found in $\tanh()$, parameterised with 4 free parameters,

$$f_{\tanh}(x) = t_1 \tanh(t_2 x + t_3) + t_4. \tag{2}$$

By introducing lower and higher limits on the potentiometer function y_{l} and y_{h}, this function can be constrained by requiring $f_{\tanh}(0) = y_{\mathrm{l}}$ and $f_{\tanh}(1) = y_{\mathrm{h}}$ resulting in

$$t_4 = y_{\mathrm{l}} - t_1 \tanh(t_3), \quad t_1 = \frac{y_{\mathrm{h}}}{\tanh(t_2 + t_3) - \tanh(t_3)}, \tag{3}$$

leaving free parameters t_2 and t_3. For a full-range law $y_{\mathrm{l}} = 0$ and $y_{\mathrm{h}} = 1$, though due to inherent terminal and wiper resistances these values will never be found from measurements of a real device.

The solid lines in Figure 3 show the fit of the $\tanh$ law to those from [8]. The $\tanh$ function with 2 free parameters in (2 - 3) were fit using the `fit` function from MATLAB 2018a's Curve Fitting toolbox, with initial parameters $t_2 = 1$ and $t_3 = -0.5$. For the anti-log characteristic the function was defined as $f^{\mathrm{Alog}}_{\tanh}(x) = \hat{f}_{\tanh}(x)$. The resultant function coefficients are shown in Table 1.

A maximum error of 4% is found in Figure 3 between the specified characteristic and fitted function for the logarithmic law, though most error falls between $\pm 2\%$. The larger error observed in the log law can be attributed to it reaching the y limits prior to the corresponding x limits. To mitigate this error, a piecewise function could be employed with the $\tanh$ function only fitting the central region, and transitioning to a different sub-function in the regions where the most error is encountered. This would however reduce the simplicity of the implementation, and other sub-functions may offer improved fit to real potentiometer device laws. The $\tanh$ function maintains applicability without additional sub-functions, offering a single function that can model each of the examined characteristics and providing this flexibility with only 2 parameters.

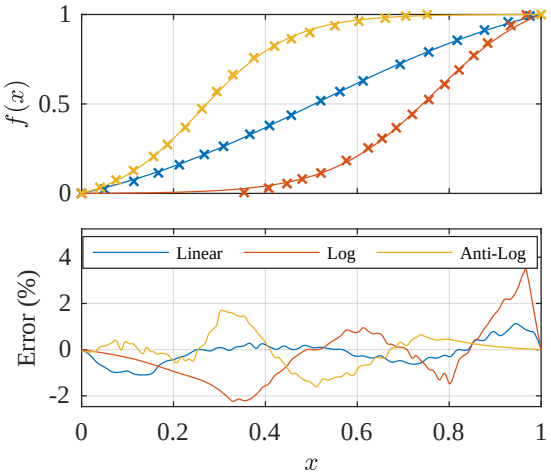

Figure 3: *Specified linear, logarithmic, and anti-logarithmic potentiometer tapers. The specified characteristic is marked by* ×*, and the fit using a* tanh *function by the solid lines. Error is shown in the lower plot.*

Table 1: *Fit parameters of the general* tanh *function to the potentiometer laws specified in [8]. Limits are given as* $y_\mathrm{l} = 0$ *and* $y_\mathrm{h} = 1$.

t	Linear	Log	ALog
t_1	0.701	0.566	0.536
t_2	1.790	4.400	5.113
t_3	−0.919	−3.380	−3.787
t_4	0.508	0.564	0.535

2.2.2. *Piecewise linear/cubic functions*

The specific potentiometers investigated within this work are of the brand Alpha, a popular brand in the building of guitar effects-pedals. Specifications for the potentiometer laws are found on their website [10]. Again the tanh function could be employed to model both linear and logarithmic laws for these specifications, however after an initial study the error peaked at 8% at the same region as observed in Figure 3, though a figure of this result is omitted for brevity. To reduce this error a piece-wise function would need to be used to capture the end-regions where the function gradient is zero. In the case that a piecewise function is required, it is a logical step to test which functions can provide the optimal fit.

The logarithmic characteristics from [10] are reproduced in Figure 4. Each law is specified by the percentage of total resistance between terminals 1 and 2 at 50 % rotation. Upon inspection of this set of characteristics there appear distinct sections with constant gradients, joined via smooth transitions. This property can be exploited through the use of a piecewise function containing linear sub-functions. Defining a linear sub-function with local lower and higher limits – $y_\mathrm{ll} = \bar{f}_\mathrm{lin}(x_\mathrm{ll})$ and $y_\mathrm{lh} = \bar{f}_\mathrm{lin}(x_\mathrm{lh})$ – results in the expression

$$\bar{f}_\mathrm{lin}(x) = \frac{y_\mathrm{lh} - y_\mathrm{ll}}{x_\mathrm{lh} - x_\mathrm{ll}}(x - x_\mathrm{ll}) + y_\mathrm{ll}, \quad \bar{f}'_\mathrm{lin}(x) = \frac{y_\mathrm{lh} - y_\mathrm{ll}}{x_\mathrm{lh} - x_\mathrm{ll}}. \quad (4)$$

The derivative of the linear sub-function is important here as there are no apparent jumps in gradient in any of the characteristics, and so the gradient of the sub-functions must match at the transitional values of the piecewise function. To achieve a match in derivatives at transitional points, 4 free parameters would be required, two for each transitional point, matching value and derivative. One such sub-function that offers this is found in a general cubic polynomial, expressed as

$$\bar{f}_\mathrm{cub}(x) = c_4 x^3 + c_3 x^2 + c_2 x + c_1, \quad (5)$$

where $c_1 - c_4$ are the cubic coefficients used to fit the sub-function $\bar{f}_\mathrm{cub}(x)$. To find values for $c_1 - c_4$ the following set of equations must be solved,

$$\bar{f}_\mathrm{cub}(x_\mathrm{ll}) = c_4 x_\mathrm{ll}^3 + c_3 x_\mathrm{ll}^2 + c_2 x_\mathrm{ll} + c_1, \quad (6)$$

$$\bar{f}_\mathrm{cub}(x_\mathrm{lh}) = c_4 x_\mathrm{lh}^3 + c_3 x_\mathrm{lh}^2 + c_2 x_\mathrm{lh} + c_1, \quad (7)$$

$$\bar{f}'_\mathrm{cub}(x_\mathrm{ll}) = 3c_4 x_\mathrm{ll}^2 + 2c_3 x_\mathrm{ll} + c_2, \quad (8)$$

$$\bar{f}'_\mathrm{cub}(x_\mathrm{lh}) = 3c_4 x_\mathrm{lh}^2 + 2c_3 x_\mathrm{lh} + c_2. \quad (9)$$

An explicit solution of this set of equations is available on the supporting online content, but is omitted here for brevity.

The choice of the linear-cubic piecewise function aims to build-in the specified behaviour of the manufacturer's characteristics. By matching the underlying structure of potentiometer characteristics, the ability to produce an accurate law from a reduced/incomplete set of measurements is improved, without needing a higher number of measurements to interpolate between.

From the specified or measured potentiometer characteristics a set of x values can be found at which the function transitions from linear to cubic (either through direct visual inspection or inspection of the gradient of the law). At these points the corresponding y values can be found by interpolating between the available data points of the characteristic, yielding a set of points that make up the piecewise function transitions.

In Figure 4, logarithmic characteristics from [10] are shown with their piecewise fit. The transitional points are approximately equal between each function, meaning that only one set of x values was required to fit the full set of characteristics. These values of x and the corresponding y values are shown in Table 2 where they are marked with their respective sub-function. A total of 7 piecewise sections were needed to match the characteristic specified by the manufacturer. The solid line in Figure 4 shows the fit of the piecewise function to the specification, the error between the two shown in the plot beneath. A peak error of 2% is found for the 15A law, with most error for each law falling within ±1%.

Figure 5 shows the characteristics as given for 'linear' laws from [10]. A similar level of accuracy can be achieved using only 5 piecewise sections as opposed to the 7 used for the logarithmic characteristics. The piecewise transitional points for each of these laws varies significantly, necessitating an individual search for the characteristic x values at which the transitions occur, found using an optimisation algorithm.

From MATLAB's Optimisation toolbox the Nelder-Mead algorithm was selected for an easy-to-implement, derivative-free algorithm to minimise the error of the function to the characteristic by changing transitional values of x [11]. Four x variables were gathered into $\boldsymbol{\theta}_x$ to use as parameters, excluding those at 0 and 1. The corresponding estimated values of $\hat{f}(x, \boldsymbol{\theta}_x)$ were then found through interpolating between the available values of y, and a complete piecewise function was assembled. The employed objective function,

$$\xi_x(\boldsymbol{\theta}_x) = \frac{1}{\eta}\sum_{n=0}^{N_\mathrm{s}} \left(y_n - \hat{f}(x_n, \boldsymbol{\theta}_x)\right)^2, \quad \eta = \sum_{n=0}^{N_\mathrm{s}} y_n^2, \quad (10)$$

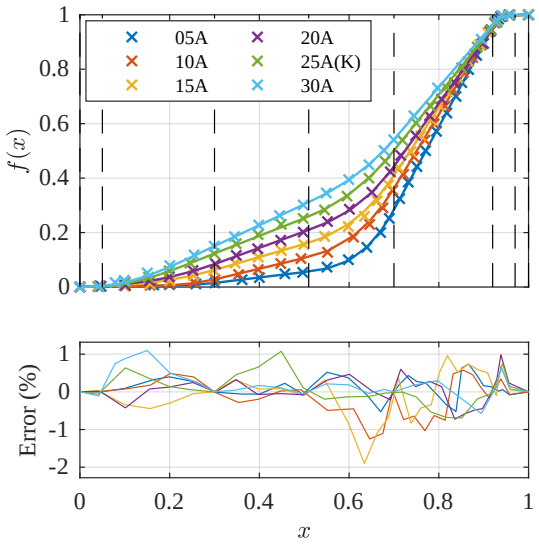

Figure 4: *Logarithmic Alpha characteristics (× marks), and fit using linear-cubic piecewise functions (solid lines). Characteristics are noted by the manufacturer's code which refer to the resistance percentage at 50% rotation. Error is shown in the lower plot. Vertical dashed lines mark the points at which the piecewise function sections change.*

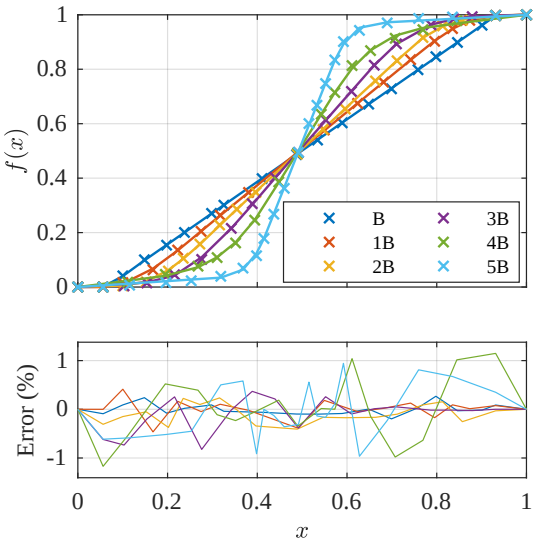

Figure 5: *Linear Alpha characteristics from (× marks), and fit using linear-cubic piecewise functions (solid lines). Characteristics are noted by the manufacturer's code. Error is shown in the lower plot. Transitions are omitted for this figure as they each fall at different values.*

enumerates the sum-squared error between the measured points of $f(x_n) = y_n$ and those found using the piecewise function with estimated transitional points $\hat{f}(x_n, \boldsymbol{\theta}_x)$. A normalisation factor η is applied to ensure that between data sets with different numbers of elements, the enumerated error would be comparable, allowing comparison between the results of the optimisation using different data sets.

Constraints are applied directly to the objective function, returning $\xi_x = 10^3$ if the constraints are not satisfied. These constraints prevent x values from exceeding domain limitations, i.e. $0 \leq \theta_x \leq 1$, and that they are incremental in value, i.e. for the jth element $\theta_x^j < \theta_x^{j+1}$.

Convergence tolerances were set at a change in value beneath 10^{-8} for both $\boldsymbol{\theta}_x$ and $\xi_x(\boldsymbol{\theta}_x)$. The resulting optimised x and corresponding y values are omitted here for brevity but can be found on the companion webpage. The solid line in Figure 5 represents the fitted piecewise function for each law, with the error between fit and specification shown in the lower plot. Peak error is approximately 1.2% with most contained within $\pm 1\%$.

With suitable functions that match the specified potentiometer laws to within 2% error, the following step is to apply this function to model the characteristic of real potentiometer devices.

2.3. Measured potentiometer characteristic

Several potentiometers were purchased from a local distributor of components for the DIY construction of guitar effects pedals. This source was selected to ensure that the potentiometers would be intended for the use in guitar effects pedals, and that they could be used to determined which laws from the presented sets in Figures 4 and 5 are used in potentiometers popular among effects-builders. The purchased potentiometers were specified to have $R_\mathrm{T} = 100\,\mathrm{k}\Omega$ ($\pm 20\%$) as this is the value of the potentiometer used in the Big Muff Pi tone stack, further discussed in §3.

Table 2: *Optimised transition points of the general cubic-linear piecewise function, fit to the logarithmic potentiometer characteristic specified in [10]. Values are rounded to 3 decimal places. 'Law' column is offset to indicate which law corresponds to each set of end-points.*

Law	x	y					
		05A	10A	15A	20A	25KA	30A
	0.000	0.000	0.000	0.000	0.000	0.000	0.000
Lin.	0.050	0.003	0.003	0.003	0.004	0.002	0.004
Cub.	0.300	0.015	0.028	0.063	0.084	0.123	0.151
Lin.	0.510	0.057	0.111	0.162	0.210	0.259	0.311
Cub.	0.700	0.284	0.363	0.410	0.443	0.501	0.542
Lin.	0.920	0.954	0.959	0.958	0.952	0.954	0.965
Cub.	0.970	0.999	0.999	1.000	1.000	0.999	1.000
Lin.	1.000	1.000	1.000	1.000	1.000	1.000	1.000

To measure the potentiometer characteristic, a measurement jig was designed with markers at 15 degree angles around a central hole where the potentiometer was fixed. The markers were placed using computer aided design/manufacturing, the jig made from FR-4 with plated copper as used in circuit-board manufacturing techniques.

Direct measurements presented here are only cursory to provide an approximate law with which to compare to those found through the following identification from I/O measurements. The potentiometer was rotated by hand to line the knob indicator to each marker, while the resistance between adjacent terminals was measured continuously with an LCR meter. Measuring the resistance at 15 degree increments over a total of 300 degrees of travel yielded 21 measurements. The obtained characteristics can be considered as suitably representative test data even in the presence of possible measurement errors, including human error when performing the manual wiper rotation and heating from continuous

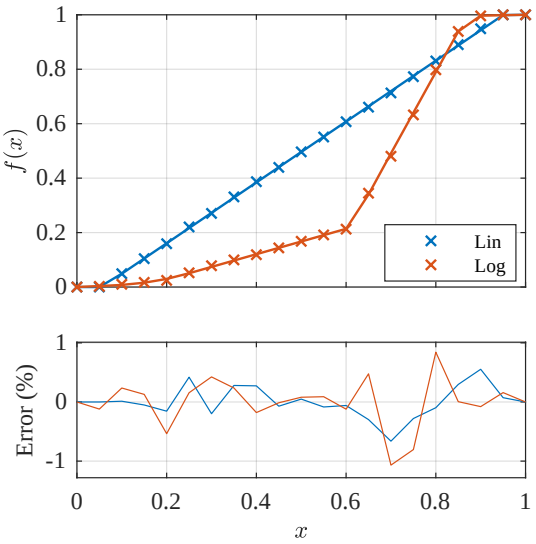

Figure 6: *Measured (× marks) and fit linear-cubic (solid lines) potentiometer laws of 1 linear and 1 logarithmic potentiometer. Error is shown in the lower plot. The laws of the two potentiometers fit with that of 'B' from Figure 5 and '15A' from Figure 4.*

Table 3: *Optimised transition points of the general cubic-linear piecewise function, fit to measurements taken of a linear and logarithmic potentiometer. Values are rounded to 3 decimal places. 'Law' column is offset to indicate which law corresponds to each set of end-points.*

	Linear		Log	
Law	x	y	x	y
Lin.	0.000	0.000	0.000	0.000
Cub.	0.050	0.000	0.071	0.005
Lin.	0.093	0.041	0.239	0.045
Cub.	0.951	1.000	0.603	0.215
Lin.	0.951	1.000	0.659	0.368
Cub.	1.000	1.000	0.850	0.939
Lin.	-	-	0.908	0.997
	-	-	1.000	1.000

driving from the LCR meter. Other physical parameters exist for the potentiometer in addition to its law, such as terminal resistance, but these were found to be of a magnitude that was impossible to measure with available equipment, and therefore likely insignificant to the identification.

Figure 6 shows the measured characteristics of both a linear and a logarithmic potentiometer, and the fit of the piecewise linear-cubic function to the measurements. A notable deviation was found from the logarithmic tapers of Figure 4, with the transition to the zero-gradient section at the maximum of the function occurring at a lower value of x. Therefore the optimisation approach used to fit the linear characteristics of Figure 5 was applied, i.e. the x positions found by optimising them and finding the corresponding values of y through interpolation of the measurement. The result is a good fit to the measurements with a peak error just over 1%. Final transitional values of the piecewise function are shown in Table 3.

3. IDENTIFYING POTENTIOMETER CHARACTERISTICS FROM I/O MEASUREMENTS

Having fit laws to characteristics obtained from both linear and logarithmic potentiometers, sufficient information is available to validate results from the law identification strategy exclusively using input/output measurements, presented in this section. The case study chosen to demonstrate this strategy is the tone stack from the Big Muff Pi, informed from the description in [12], with the schematic shown in Figure 7. In simple terms, the potentiometer in the Big Muff Pi tone stack blends between a low pass formed between R_1 and C_2, and a high pass filter formed by C_1 and R_2. Both linear and logarithmic potentiometers will be used to demonstrate the capability of the identification strategy to succeed independent of potentiometer law.

The tone stack was assembled on a breadboard to enable direct measurement of each component prior to the measurement of the circuit's transfer function. Use of a breadboard also facilitates the measuring of both linear and logarithmic potentiometers to demonstrate the identification procedure for the two most common laws. Specified and directly measured component values can be found in Table 4.

Only one potentiometer is present in the circuit. The presented method should allow for independent identification of multiple potentiometers by setting all but the potentiometer of interest at a known position, at 0 or 300 degrees rotation, resulting in $N \times M$ independent identifications where N is the number of positions per potentiometer and M the number of potentiometers. This property cannot be demonstrated using this circuit, but can be inferred as only one variable, a single potentiometer position, would be changed in between each measurement.

To begin identifying the potentiometer laws from input/output measurements, one must start with estimates of the component values, obtained from schematics or other identification strategies. Should the component values be highly accurate, the input/output measurements should theoretically be matched when the potentiometer is at either extreme of its rotational travel. At these points the values of y are assumed known. The accuracy of the fit achieved at these limits will provide some indication of how accurately the law can be retrieved.

The selection of a linear case study provides several desirable traits: the circuit model can be represented using a transfer function which requires only a few data points to capture a large frequency range, and issues of nonlinear behaviour such as aliasing are avoided. The tone stack is modelled as a transfer function derived using Modified Nodal Analysis [13]. The resultant function is of the form

$$H(j\omega) = \frac{b_3(j\omega)^3 + b_2(j\omega)^2 + b_1 j\omega}{a_4(j\omega)^4 + a_3(j\omega)^3 + a_2(j\omega)^2 + a_1(j\omega)^1 + a_0}. \tag{11}$$

Complete coefficients are omitted due to their complexity, but MATLAB code for calculating the transfer function is available on the companion webpage. Figure 8 shows the simulated amplitude responses of the Big Muff Pi's tone stack with the potentiometer at each end of its travel: presuming these responses to be accurate the challenge then lies in measuring intermediate responses and identifying the corresponding values of $f(x)$.

Table 4: *Component values of the Big Muff Pi tone stack: specified values and the values directly measured from the circuit using an LCR meter.*

	Unit	Specified	Measured
R_1	kΩ	39.000	39.080
R_2	kΩ	22.000	21.950
R_T	kΩ	100.000	94.940 (lin) / 98.140 (log)
R_o	kΩ	100.000	99.978
C_1	nF	4.700	4.698
C_2	nF	10.000	9.470
C_3	nF	100.000	98.010
C_d	pF	100.000	33.227

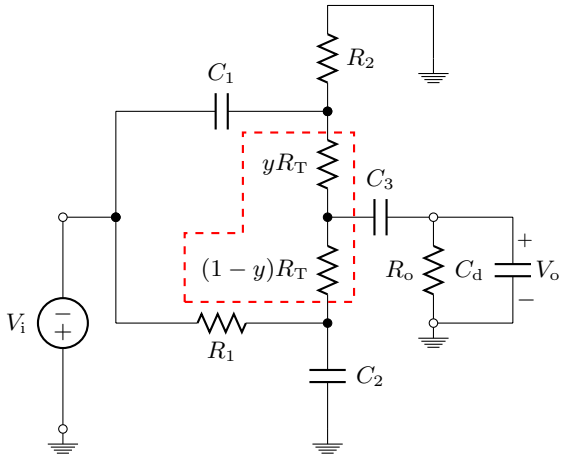

Figure 7: *Schematic of the Big Muff Pi tone stack with potentiometer marked by red line. C_d is the input capacitance of the measurement equipment used.*

3.1. Identification strategy

The identification strategy proposed in this work identifies a potentiometer's characteristic from input/output measurements of a circuit. A series of optimisations are performed, only operating on a single value of x at a time. Values of $y = f(x)$ are estimated at each point, thus identifying the potentiometer characteristic. To perform such optimisations, an objective function is required which compares the measurements of the circuit to the equivalent data from the model, enumerating the error between circuit and model.

Considering the linear case exhibited by the Big Muff Pi tone stack, the input/output measurements can be condensed into the form of a transfer function. Due to the limitations of the measurement equipment (further discussed in Section 3.2) only the amplitude response of the transfer function is used, with phase information discarded. From this information the objective function was constructed, for an estimated value of $y = f(x)$,

$$\xi_\mathrm{io}(y) = \frac{1}{\sum_{n=0}^{N_\mathrm{s}-1}|H(j\omega_n)|^2}\sum_{n=0}^{N_\mathrm{s}-1}\left(|H(j\omega_n)| - |\hat{H}(j\omega_n, y)|\right)^2, \tag{12}$$

where the operator $|\cdot|$ indicates the magnitude of a complex value. Frequencies of the transfer function are specified using ω_n, where n indicates index of the discrete frequency selected to be included in the measurement data.

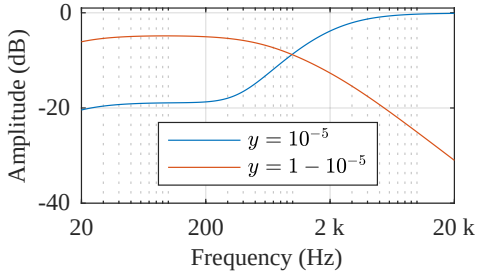

Figure 8: *Amplitude responses of the Big Muff Pi tone stack with the potentiometer at extreme ends of its rotational travel.*

The optimisation algorithm chosen to minimise the value of $\xi_\mathrm{io}(y)$ was that of `fminsearch` from MATLAB's optimisation toolbox, specifically the Nelder-Mead simplex algorithm. Convergence conditions were again set to be a change in y or ξ_io less than 1×10^{-8}. Initial experiments using simulated I/O measurements demonstrated successful identification of the potentiometer characteristics to within $10^{-5}\%$ of the accurate value.

3.2. Measurement procedure

Among various possible valid measurement approaches to find the transfer function of the Big Muff Pi tone stack, a multi-sine excitation signal was chosen, expressed as

$$V_\mathrm{i} = V_\mathrm{p}\sum_{d=d_\mathrm{l}}^{d_\mathrm{u}} A_d \cos(2\pi d f_0 n T + \phi_d), \quad n = 0, \ldots, N_\mathrm{s}. \tag{13}$$

The integer values of d are limited to contain sinusoidal components at multiples of $f_0 = f_\mathrm{s}/N_\mathrm{s}$ between the lower and upper limits d_l and d_u. Phase terms ϕ_d are specified as in [14], i.e.

$$\phi_d = -2\pi\sum_{l=1}^{d-1}(d-l)A_d, \quad d = d_\mathrm{l}, d_\mathrm{l}+1, ..., d_\mathrm{u}. \tag{14}$$

which requires that $1 = \sum_{d=d_\mathrm{l}}^{d_\mathrm{u}} A_d$. Individual amplitude components allow a frequency-domain weighting to be applied which can be used to maximise the signal-to-noise ratio, but in this case were set to be $A_\mathrm{d} = 1/(d_\mathrm{u} - d_\mathrm{l})$.

Finally the value of V_p is selected such that the peak voltage of the resultant signal is normalised to a chosen peak voltage typically as defined by the measurement equipment.

To produce a transfer function from the measured output of the circuit, the input is deconvolved from the output signal by performing an element-wise division in the frequency domain.

An excitation signal was designed with frequencies between 1 Hz − 20.1 kHz, i.e. $f_0 = 1$, $d_\mathrm{l} = 1$ and $d_\mathrm{h} = 20100$. The measured frequency range was measured outside of the anticipated required range in case this information was important to the identification, though the range is later restricted to 20 Hz – 20 kHz. The limitations of the analogue input was 2 V which was used to find the value of V_p. The signal was repeated 60 times and averaged to one period to reduce stochastic noise.

The measurement equipment used is a National Instruments myDAQ. Previous experiments with Data Acquisition devices and identification have shown that any errors in the phase response can severely effect accuracy in the identification procedure [4]. Upon

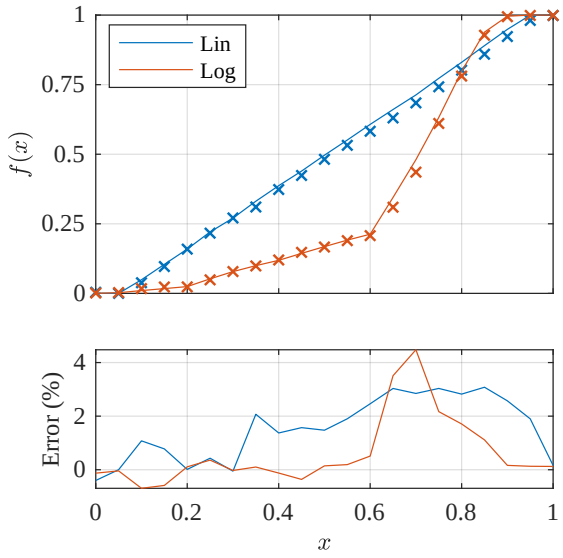

Figure 9: *Potentiometer laws as directly measured (solid line) and estimated from I/O measurements (× marks), and error between the two sets presented beneath.*

detection of phase error by testing the unloaded I/O response, it was decided that the phase response should be omitted from the identification data.

A notable capacitance was measured across the input to the myDAQ, noted as C_d in Table 4. This capacitance was included in the circuit model to incorporate any effect it may have on the measured transfer functions. The measured value of C_d was found by driving a series impedance of $2\,\mathrm{M\Omega}$ with a multi-sine signal, and measuring the cutoff frequency of resulting RC low pass filter at approximately $2.395\,\mathrm{kHz}$.

Measurements were taken from 21 positions along the rotational axis of both the linear and logarithmic potentiometers (15 degree rotations from 0-300 degrees). The amplitude response of each of the measured transfer functions was then used to estimate the value of y at each position. To minimise computational expense during optimisation, the transfer function data was downsampled from 20.1×10^3 data points to 512 points spaced logarithmically between 20 Hz and 20 kHz, each point rounded to the nearest integer such that it corresponds to a measured value, not requiring interpolation. Removing duplicate entries that occur at low frequencies results in a unique set of 469 amplitudes/frequencies.

4. RESULTS

Optimisation was applied as described in Section 3.1, using the Nelder-Mead algorithm and the objective function described in (12). Convergence was achieved successfully from each optimisation.

The identified potentiometer laws for both linear and logarithmic potentiometers are shown in Figure 9, with the solid line representing the directly measured law and the × marking the values estimated using the identification strategy. Error between the sets peak at approximately 4.5 % for the logarithmic characteristic and 3 % for the linear characteristic.

Illustrated for both potentiometer laws in Figure 10 are the measured and identified amplitude responses of the Big Muff Pi tone stack. This serves to provide one way of attributing error but also as a source of validation. Inspecting the x values of high error in Figure 9 it is clear that there is not an anomalous amount of error in the fit to the amplitude response at corresponding values. Consistent accuracy from identified amplitude responses but increasing error in the identified potentiometer characteristic points towards the error being introduced by device heating/human error during measurement.

As a form of validation, the fit to measurements demonstrated in Figure 10 is accurate to within 1 dB across all measurements, indicating that the tone stack filtering effect is captured over the the full wiper range.

5. CONCLUSION

This work has focused on the modelling and identification of potentiometer laws without device disassembly. Two functions were proposed to model potentiometer characteristics as found in specifications and from measurements, a $\tanh()$ based function and a piecewise linear-cubic function. The latter was used to model the laws of Alpha potentiometers as given by both specifications and measurements within 2% error.

Identification of the potentiometer characteristics from I/O measurements of the device was tested on a linear subcircuit of the Big Muff Pi: the tone stack. Identification exclusively using the amplitude response of the subcircuit was shown to be possible, with the results of the identification retrieving both linear and logarithmic potentiometer characteristics to within 4.5% error.

It is likely that some of this 4.5% error has been introduced by device heating and/or human error. Increasing the precision and repeatability of the measurements could be achieved by the design of an automated mechatronic system that would simultaneously rotate the potentiometer wiper and perform measurements. One such solution might involve e.g. a stepper motor to control the potentiometer and a pulsed measurement system to control the variation in resistance caused by changes in temperature.

For those seeking a fast method of determining the orientation and approximate law of a potentiometer, a complete set of 21 points is not required. Assuming $f(0)$ and $f(1)$ are known, from e.g. parameter estimation as in [4], only one additional measurement at $f(0.5)$ is sufficient to differentiate between linear and logarithmic/anti-logarithmic. A further measurement at e.g. $f(0.25)$ or $f(0.75)$ would then enable differentiation between orientations of the potentiometer and also logarithmic and anti-logarithmic laws.

The anticipated application of this identification strategy is for complete, nonlinear audio circuits. Elements that may cause issues in the identification include nonlinear behaviour, and effects for which potentiometers control behaviour that is difficult to measure, e.g. LFO rate in a phasor effect. The low-data point amplitude response facilitates fast identification, which has significant benefits with regard to rapid design and refinement of the identification process. Time-based and/or nonlinear effects would prevent this selection and therefore demand a search for a suitable, similarly efficient, objective function. For example, a gain control may use the Total Harmonic Distortion of the output waveform when driven by a sinusoid, or for a delay length control, the time between repeats when driven by a pulse-type signal. Each control type requires individual attention, but due to the monotonic nature of the studied potentiometer laws, and as each potentiometer can be identified independently, each position should yield a unique measured value, so long as the objective function is well-chosen.

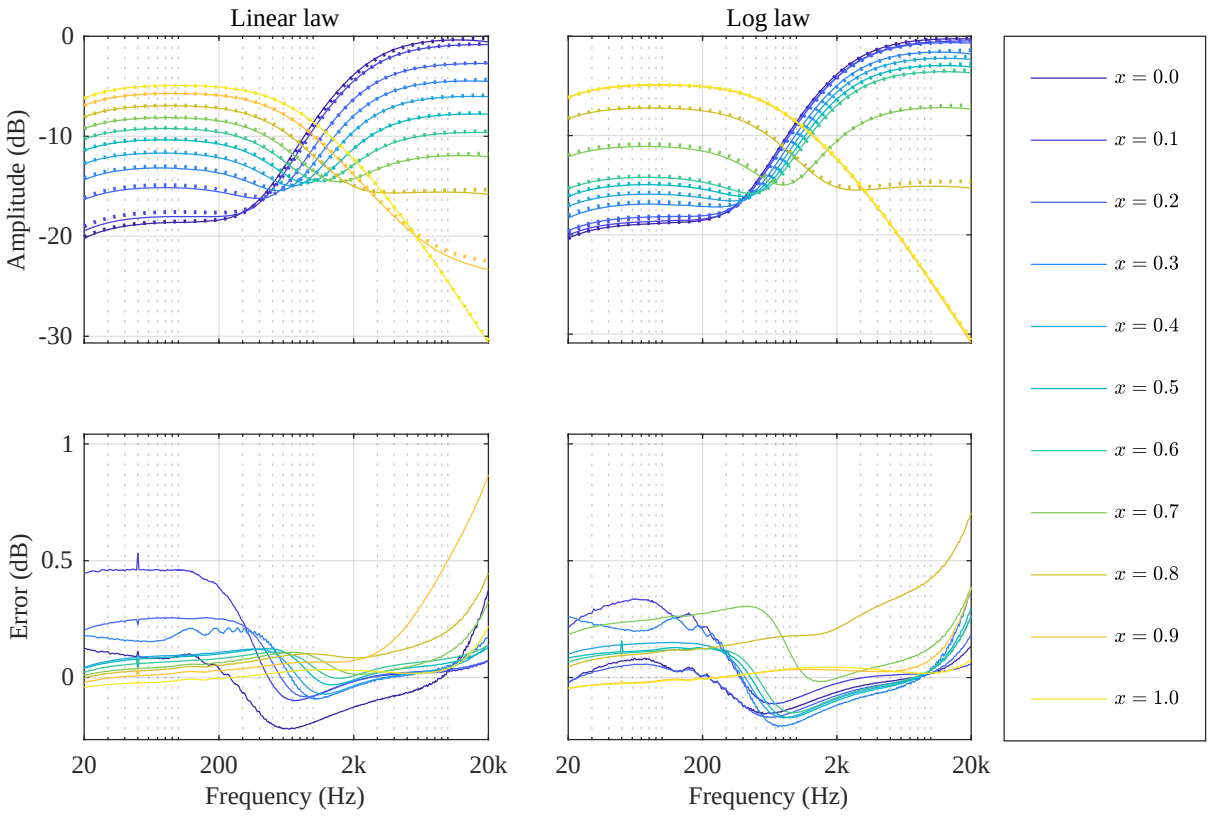

Figure 10: *Estimated (dotted) and measured (solid) amplitude responses of the Big Muff tone stack, with error in decibels shown below. Only 11 of the 21 measured amplitude responses are shown to improve clarity of the figure.*

6. REFERENCES

[1] Felix Eichas and Udo Zölzer, "Gray-Box Modeling of Guitar Amplifiers," *Journal of the Audio Engineering Society*, vol. 66, no. 12, pp. 1006–1015, Dec. 2018.

[2] Antonin Novak, Pierrick Lotton, and Laurent Simon, "Synchronized Swept-Sine: Theory, Application, and Implementation," *Journal of the Audio Engineering Society*, vol. 63, no. 10, pp. 786–798, Nov. 2015.

[3] Lamberto Tronchin and Vanna Lisa Coli, "Further Investigations in the Emulation of Nonlinear Systems with Volterra Series," *Journal of the Audio Engineering Society*, vol. 63, no. 9, pp. 671–683, Oct. 2015.

[4] Ben Holmes, *Guitar Effects-Pedal Emulation and Identification*, Ph.D. thesis, Queen's University Belfast, June 2019.

[5] Miller Puckette, *The Theory and Technique of Electronic Music*, World Scientific Publishing Co. Pte. Ltd., 2007.

[6] Oliver Larkin, Alex Harker, and Jari Kleimola, "iPlug 2: Desktop Plug-in Framework Meets Web Audio Modules," in *Proceedings of the 4th Web Audio Conference*, Sept. 2018.

[7] Ankit Rohatgi, "WebPlotDigitizer," https://automeris.io/WebPlotDigitizer/, Apr. 2019.

[8] Carl David Todd, *The Potentiometer Handbook: Users' Guide to Cost-Effective Applications*, McGraw-Hill, New York, 1975.

[9] U.S.A. Department of Defense, "Military specification MIL-PRF-94G: Resistors, variable, composition general specification for," Tech. Rep., Aug. 2011.

[10] Alpha Products, "Taper Curves for our Potentiometers," http://www.alphapotentiometers.net/html/taper_curves.html, 2014.

[11] Jeffrey C. Lagarias, James A. Reeds, Margaret H. Wright, and Paul E. Wright, "Convergence properties of the Nelder–Mead simplex method in low dimensions," *SIAM Journal on Optimization*, vol. 9, no. 1, pp. 112–147, 1998.

[12] Electrosmash, "Big Muff Pi Analysis," https://www.electrosmash.com/big-muff-pi-analysis.

[13] Chung-Wen Ho, Albert E. Ruehli, and Pierce A. Brennan, "The Modified Nodal Approach to Network Analysis," *IEEE Transactions on Circuits and Systems*, vol. 22, no. 6, pp. 504–509, 1975.

[14] Manfred Schroeder, "Synthesis of low-peak-factor signals and binary sequences with low autocorrelation (Corresp.)," *Information Theory, IEEE transactions on*, vol. 16, no. 1, pp. 85–89, 1970.